Thouless energy and multifractality across the many-body localization transition

Maksym Serbyn, Z. Papić, and Dmitry A. Abanin

Phys. Rev. B **96**, 104201 — Published 6 September 2017

DOI: 10.1103/PhysRevB.96.104201

Thouless energy and multifractality across the many-body localization transition

Maksym Serbyn[1,2], Z. Papić[3], and Dmitry A. Abanin[4]
[1] *Department of Physics, University of California, Berkeley, California 94720, USA*
[2] *Institute of Science and Technology (IST) Austria, Am Campus 1, 3400 Klosterneuburg, Austria*
[3] *School of Physics and Astronomy, University of Leeds, Leeds, LS2 9JT, United Kingdom and*
[4] *Department of Theoretical Physics, University of Geneva, 24 quai Ernest-Ansermet, 1211 Geneva, Switzerland*
(Dated: August 16, 2017)

Thermal and many-body localized phases are separated by a dynamical phase transition of a new kind. We analyze the distribution of off-diagonal matrix elements of local operators across this transition in two different models of disordered spin chains. We show that the behavior of matrix elements can be used to characterize the breakdown of thermalization and to extract the many-body Thouless energy. We find that upon increasing the disorder strength the system enters a critical region around the many-body localization transition. The properties of the system in this region are: (i) the Thouless energy becomes smaller than the level spacing; (ii) the matrix elements show critical dependence on the energy difference; and (iii) the matrix elements, viewed as amplitudes of a fictitious wave function, exhibit strong multifractality. This critical region decreases with the system size, which we interpret as evidence for a diverging correlation length at the many-body localization transition. Our findings show that the correlation length becomes larger than the accessible system sizes in a broad range of disorder strength values, and shed light on the critical behavior near the many-body localization transition.

I. INTRODUCTION

The understanding of thermalization and its breakdown in isolated, interacting many-body systems is a fundamental and long-standing problem in quantum statistical mechanics. The recent strong theoretical interest in this problem is fueled by the experimental realization of synthetic, tunable systems of ultra-cold gases, where real-time quantum dynamics can be probed.[1]

The fact that isolated ergodic systems, prepared in a non-equilibrium state, reach thermal equilibrium is understood as a consequence of the Eigenstate Thermalization Hypothesis (ETH).[2–4] The ETH states that the mean values of the observables, evaluated in individual eigenstates of an ergodic system, coincide with the values given by the microcanonical ensemble, up to corrections that rapidly decay with the system size. In addition, to describe the approach towards equilibrium, the ETH makes assumptions about the off-diagonal matrix elements of the operators corresponding to physical observables.[5,6]

Recently, many-body localization (MBL) has attracted much interest as a mechanism by which the system can break ergodicity and avoid thermalization.[7–10] MBL phases exhibit the expected characteristics of a non-ergodic system: they violate the ETH, have area-law entanglement[11–13] and Poisson spectral statistics. These, as well as dynamical properties – a logarithmic spreading of entanglement[14–16] and time dependence of local observables following a quench[17] – have been understood as a consequence of the emergence of local integrals of motion in MBL phases.[12,13,18,19]

Generally, a quantum system is expected to exhibit a phase transition between the ergodic and localized phase as the disorder strength is varied. The Anderson localization transition (ALT) for non-interacting particles can be characterized using the wave function of a system in real space. In the critical region, this wave function becomes multifractal. As one approaches the ALT from the metallic side, the critical region can be identified using the Thouless energy – the central concept in the scaling theory of the Anderson localization.[20] In the critical region preceding the ALT, the Thouless energy, which sets the correlations between wave functions at different energies, becomes comparable to the (single-particle) level spacing.

Similarly, the many-body localization transition (MBLT) can be driven by changing the disorder strength in an interacting many-particle system. While a complete theory of such a transition is lacking, phenomenological RG[21,22] and numerical[23–29] studies have uncovered several fascinating properties in one-dimensional models, notably the sub-diffusive transport on the ergodic side of the MBLT in the XXZ spin chain. While the phenomenological RG approach suggests the existence of a broad critical region surrounding the MBLT, it is not clear how this region can be identified using numerical studies of finite size microscopic models.

In this work, inspired by the successful description of the ALT using the Thouless energy and real-space wave functions, we introduce and study similar concepts for the MBLT. In particular, we utilize the relation between the matrix elements $O_{\alpha\beta} = \langle\beta|\hat{O}|\alpha\rangle$, of a local observable $\hat{O}$ between the many-body eigenstates $|\alpha\rangle, |\beta\rangle$, and the dynamical properties of the system. The Thouless energy is defined as the maximum energy difference, $E_\alpha - E_\beta$, of the eigenstates $|\alpha\rangle, |\beta\rangle$ for which the matrix element $O_{\alpha\beta}$ remains constant. This definition may be viewed as a generalization of the definition of Thouless energy from the energy structure of wave functions overlap[30,31] to the

many-body case.

While the Thouless energy is expected to vanish in the thermodynamic limit, in the finite size system it physically corresponds to the inverse time for the spreading of a local perturbation, introduced by the operator $\hat{O}$, throughout the volume of the system. In addition, treating the matrix elements $O_{\alpha\beta}$ as amplitudes of a (fictitious) wave function obtained by acting with a local operator $\hat{O}$ on an eigenstate $|\alpha\rangle$, we study its statistics using the fractality toolbox developed in the context of ALTs.[32–36]

Our main findings can be summarized as follows. Upon approaching the MBLT from the ergodic side by increasing the strength of the disorder, we find that the Thouless energy, extracted from the energy dependence of the matrix elements, rapidly decreases for a system of fixed size L. The system size for which the Thouless energy becomes comparable to the many-body level spacing is interpreted as a correlation length $\xi(W)$. This correlation length grows as the system approaches the MBLT, consistent with its divergence at the MBLT. For systems of size smaller than $\xi(W)$, we observe signatures of critical behavior: the matrix elements at a fixed energy difference acquire broad distribution, so that typical and average matrix elements exhibit *qualitatively* different behavior with energy difference. In addition, consistent with the breakdown of self-averaging, we find multifractal behavior of the matrix elements $O_{\alpha\beta}$.

The remainder of the paper is organized as follows. In Section II, we introduce the spectral function as a convenient quantity to describe the energy dependence of the matrix elements and discuss its relation to the dynamics of the system. The models and numerical methods are introduced in Section III. Our results for the Thouless energy and the spectral function are presented in Section IV. Section V discusses the fractal statistics of the matrix elements. Finally, in Section VI we summarize and discuss our results in the context of earlier numerical studies and the theoretical description of the MBLT. Additional numerical data is presented in Appendices.

II. FROM MATRIX ELEMENTS TO DYNAMICS

Our main focus throughout this paper is to study the properties of matrix elements

$$O_{\alpha\beta} = \langle\beta|\hat{O}|\alpha\rangle \tag{1}$$

of some local observable $\hat{O}$ between the system's eigenstates $|\alpha\rangle, |\beta\rangle$. In this Section, we first show that the matrix elements (1) contain information about the dynamical properties of the system. We are interested in generic properties of the system, which will be shown to be insensitive to the specific choice of the observable $\hat{O}$.

In order to study the dependence of matrix elements on the energy difference, we introduce a function

$$f^2(\omega) = e^{S(E)}\langle|O_{\alpha\beta}|^2\delta(\omega-(E_\beta-E_\alpha))\rangle, \tag{2}$$

where $S(E)$ is the thermodynamic entropy at the average energy $E = (E_\alpha + E_\beta)/2$. Since we will focus on the behavior near the middle of the many-body spectrum, we suppress the average energy E in this definition. The average here is performed both over eigenstates near the middle of the spectrum, and over disorder realizations.

The definition (2) is inspired by the ETH ansatz for a matrix element in an ergodic system,[6]

$$O_{\alpha\beta} = \mathcal{O}(E)\delta_{\alpha\beta} + e^{-S(E)/2}f(E,\omega)R_{\alpha\beta}, \tag{3}$$

where the first term on the right hand side corresponds to the expectation value of $\hat{O}$. The second term, describing off-diagonal matrix elements, is a product of random numbers $R_{\alpha\beta}$ with zero mean and unit variance, and a smooth function $f(E,\omega)$ that depends on the energy difference $\omega = E_\alpha - E_\beta$ and average energy E. The ansatz in Eq. (3) has been tested numerically in several models.[37–40] Function $f(\omega)$ in Eq. (2) coincides with the smooth function $f(E,\omega)$ used in Srednicki's ansatz under the assumptions that the δ-function is broadened on a scale larger than the many-body level spacing, and that $R_{\alpha\beta}$ averages out.

Function $f^2(\omega)$ encodes two important physical characteristics of our system. Neglecting the variation of $S(E)$ near the middle of the many body spectrum $E \approx 0$, one can show that $f^2(\omega)$ coincides with the average spectral function for states with $E_\alpha \approx 0$, measurable in a tunneling or absorption experiment. Furthermore, the Fourier transform of $f^2(\omega)$ determines the time dependence of the connected correlation function[40]

$$F_\alpha(t) = \langle\alpha|\hat{O}(t)\hat{O}(0)|\alpha\rangle_c. \tag{4}$$

Provided the $f(\omega)$ is a smooth function and its fluctuations average out, this correlator is equal to

$$F_\alpha(t) \approx \int_{-\infty}^{\infty} d\omega\, e^{-i\omega t} f^2(\omega). \tag{5}$$

Function $F_\alpha(t)$ enters the generalization of the Fluctuation-Dissipation Theorem.[37,40] If the operator $\hat{O}$ corresponds to the density of a conserved quantity, $F(t)$ gives the return probability and can be related to the conductivity of a system via the Einstein relation.[23]

The Fourier transform (4) can be used to infer the effect of $f^2(\omega)$ on the real-time dynamics in the ergodic phase. In particular, on time scales longer than the local hopping or the exchange scale (denoted as $J_{\rm loc}$ in what follows), $t > 1/J_{\rm loc}$, the return probability decays as a power-law in time, $F(t) \propto 1/t^\gamma$, with the exponent $\gamma = 1/2$ for the case of diffusion and $\gamma > 1/2$ for subdiffusive dynamics. This implies that the Fourier transform of the return probability, $f^2(\omega) \propto 1/\omega^\phi$, with the exponent $\phi = 1-\gamma$.

The dynamics saturates when an excitation explores the full system. Assuming that the operator corresponds to the injection of conserved quantity, the saturation value is inversely proportional to the system size, giving the saturation time $1/t^\gamma \propto 1/L$. From here, we

expect that the real-time dynamics saturates at times $t_* \propto L^{1/\gamma}$. Saturation of $F(t)$ at long times corresponds to a constant value of $f^2(\omega)$ at energies below the Thouless energy $E_{\rm Th} = 1/t_* \propto L^{-1/\gamma}$. The featureless form of $f^2(\omega)$ for $\omega < E_{\rm Th}$ is natural since for times longer than t_*, a local excitation explores the full system, dimensionality is effectively lost and the system is described by the random matrix theory.

The above results can be summarized as the following asymptotic behavior:

$$f^2(\omega) \propto \begin{cases} \text{const}, & \omega \le E_{\rm Th}, \\ 1/\omega^{\phi}, & E_{\rm Th} \ll \omega \ll J_{\rm loc}, \end{cases} \tag{6}$$

with the Thouless energy and the exponent being determined by γ that defines the (sub)diffusive dynamics:

$$E_{\rm Th} \propto L^{-1/\gamma}, \qquad \phi = 1 - \gamma. \tag{7}$$

This scaling of $E_{\rm Th}$ with $\gamma = 1/2$ has been verified for the clean one-dimensional model of interacting hard-core bosons in a parabolic trap in Ref. 40. In the context of disordered systems, recently Ref. 41 used the unusual behavior of the level compressibility as evidence for the existence of the Thouless energy that is much larger than level spacing in the ergodic phase of the XXZ spin chain.

Below we present a systematic study of $f^2(\omega)$ across MBLT in two different models. We note that various aspects of the function $f^2(\omega)$ in models with MBLT were considered before. In particular, the spectral function in the MBL phase was studied in Ref. 42. The function $f^2(\omega)$ was related to the behavior of the level statistics near the MBLT.[43] Finally, Ref. 44 numerically studied the fluctuations of nearest neighbor matrix elements (which is equivalent to $f^2(\omega)$ for ω equal to the many-body level spacing), connecting these to the real-time dynamics.

III. MODELS AND METHODS

In this paper we consider two models of disordered spin chains which realize a MBLT. The first model is the familiar 1D random-field spin-1/2 Heisenberg model,[10]

$$H = \frac{1}{2}\sum_{i=1}^{L} \boldsymbol{\sigma}_i \cdot \boldsymbol{\sigma}_{i+1} + \sum_{i=1}^{L} h_i \sigma_i^z, \tag{8}$$

where σ_i^α is the Pauli matrix $\alpha = x, y, z$ on site i. Periodic boundary conditions imply $\sigma_{L+1}^\alpha = \sigma_1^\alpha$. The phase of this model depends on the disorder strength W that sets the width of the uniform distribution of the random field $h_i \in [-W; W]$. For example, when $W > W_c$, the model (8) was demonstrated to be in the "fully" MBL phase[10,45,46] (i.e., nearly all of the eigenstates of the model are localized). At weaker disorder, $W < W_c$, the eigenstates in the center of the many-body band become delocalized, and the mobility edge appears. Previous studies determined the location of the transition to be $W_c \approx 3.75$, and found that the transport is *subdiffusive* on the delocalized side of the transition.[23–29] Refs. 25 and 29 suggested subdiffusive behavior down to very small disorder, while Ref. 27 reported a transition to normal diffusion at a moderate disorder

The second model we consider is the transverse field Ising model with a disordered longitudinal field. This model was studied earlier,[47] and also it was considered in the context of Floquet dynamics.[48] Here, instead of the Floquet unitary operator, we study the Hamiltonian version of this model:

$$H_{\rm Ising} = \sum_{i=1}^{L} g\Gamma\sigma_i^x + \left(h + g\sqrt{1-\Gamma^2}G_j\right)\sigma_i^z + \sum_{i=1}^{L}\sigma_i^z\sigma_{i+1}^z, \tag{9}$$

where G_j are independent normal-distributed random numbers, and we assumed periodic boundary conditions, $\sigma_{L+1}^\alpha = \sigma_L^\alpha$. We fix the values of the coupling constants $g = 0.9$ and $h = 0.8$,[48] which control the strength of the (constant) transverse and longitudinal fields. We expect the model to show similar behavior for other values of these couplings. The control parameter is $\Gamma \in [0, 1]$, which sets the disorder strength. Small values of Γ correspond to strong disorder, while when Γ approaches one, disorder effectively disappears from the Hamiltonian (9). In contrast to the XXZ spin chain, there is no conservation of the total magnetization in the Ising model; moreover, the longitudinal field breaks the integrability of this model even at zero disorder. Thus, the Ising model is more generic than the XXZ model, due to the lack of U(1) symmetry, and its ergodic phase is more robust because it is not affected by a nearby integrable point.

In Fig. 1 we verify that the model (9) has a MBLT which occurs at $\Gamma_c \approx 0.4$. The plot shows the mean ratio

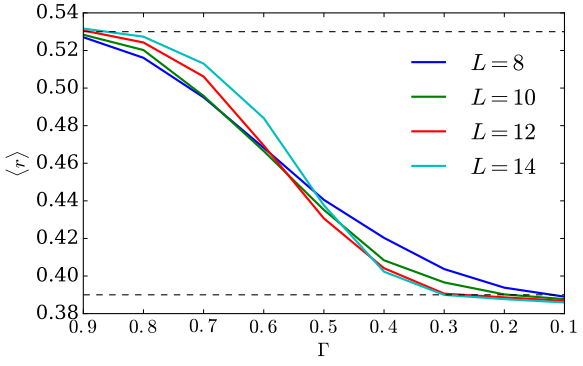

Figure 1. Mean ratio of energy level spacings $\langle r \rangle$ in the Ising model (9) as a function of disorder strength Γ. The ratio interpolates between its values for the Wigner-Dyson (top dashed line) and Poisson distributions (bottom dashed line). The crossing between the curves drifts towards stronger disorder (smaller values of Γ) with increasing the system size, similar to the XXZ spin chain.[10]

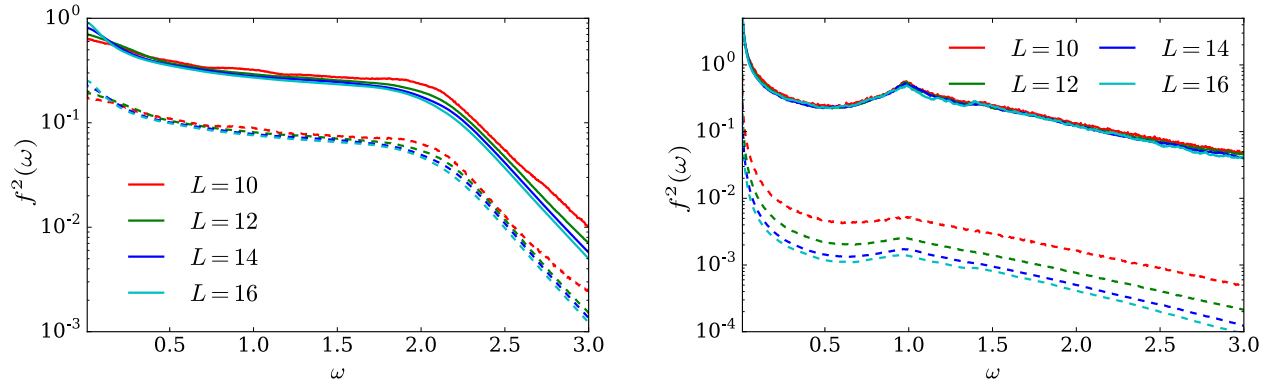

Figure 2. Spectral function $f^2(\omega)$ in the XXZ model. Left: At weak disorder ($W = 0.5$), $f^2(\omega)$ for different system sizes collapse onto each other for both average (solid lines) and typical (dashed) curves. Right: For disorder $W = 2.75$, the collapse breaks down for dashed lines, which correspond to the typical spectral function. The Thouless energy, that was visible in the left panel at small ω, now cannot be resolved, and solid lines collapse onto each other in the full range.

of the adjacent level spacings $\delta_n = E_{n+1} - E_n$,

$$\langle r \rangle = \left\langle \frac{\min(\delta_n, \delta_{n+1})}{\max(\delta_n, \delta_{n+1})} \right\rangle. \tag{10}$$

This quantity is known to be a robust indicator of thermalization and localization.[10] In the limits of weak and strong disorder, $\langle r \rangle$ approaches the values 0.53 and 0.39, respectively, which correspond to Wigner-Dyson and Poisson statistics. The crossing between the curves for $L = 12$ and $L = 14$ spin chains suggests that the MBLT happens near $\Gamma_c \approx 0.4$.

In order to study the properties of the matrix elements and to extract the Thouless energy, we will mostly work with the operator $\hat{O} = \sigma_i^z$ with $i = 1$. We do not perform averaging over different positions of the operator, although such averaging can potentially increase statistics. In Appendices we consider spectral function of local spin flip operator to demonstrate that the choice of the operator does not qualitatively affect our results.

In order to extract properties of the matrix elements in XXZ spin chain, we use exact diagonalization (ED) for chains with $L = 10, \ldots, 16$ spins and shift-invert (SI) algorithm from PETSc/SLEPc package[49] with MUMPS eigensolver for $L = 18,\ 20$ spins. We consider states in the total $\sum_i \sigma_i^z = 0$ sector near the energy $E = 0$, which lies in the middle of the spectrum. For the XXZ model, we use between 10^4 and 100 disorder realizations for $L = 10, \ldots, 20$ spins. With the SI algorithm we obtain 10^3 eigenvectors closest to the target energy $E = 0$. For the Ising model, we use ED for chains up to $L = 14$ spins and averaging over 5000 to 100 disorder realizations for $L = 10, \ldots, 14$ spins.

IV. THOULESS ENERGY AND THE DECAY OF THE RETURN PROBABILITY

A. Global form of the spectral function

We start by considering the function $f^2(\omega)$ defined in Eq. (2). We evaluate this function for operator $\hat{O} = \sigma_1^z$ in the XXZ model. The averaging in Eq. (2) is performed both over eigenstates α, β and disorder realizations. In addition, we also consider log-averaged ("typical") spectral function, defined as

$$[f^2(\omega)]_{typ} = \exp(\langle \ln f^2(\omega) \rangle), \tag{11}$$

where the brackets denote averaging over disorder and eigenstates; see Appendix A for additional details on the numerical procedure.

We find that for all values of the disorder $f^2(\omega)$ weakly depends on the system size unless ω is very small. Three different regimes can be identified in Figure 2: at large $\omega \geq J_{\rm loc}$ where $J_{\rm loc}$ is of order one, the spectral function decays exponentially due to locality of the considered operator.[50] In the intermediate frequency range there is a power-law decay, most prominent in the right panel of Fig. 2. Finally, at the very small ω the curves for different systems do not collapse onto each other (see the left panel of Fig. 2). This is manifestation of the Thouless energy, which we discuss below. As we show below, at stronger disorder $W = 2.75$ (closer to the MBLT), the Thouless energy becomes smaller than the level spacing, and hence the solid lines in the bottom panel of Fig. 2 perfectly collapse onto each other down to the smallest value of ω. At the same time, the log-averaged spectral function (dashed lines) changes with the system size suggesting onset of the broad distributions of matrix elements discussed below.

To access the properties of $f^2(\omega)$ at small frequencies, we plot it as a function of ω/Δ for both XXZ and Ising models in Fig. 3. Here the many-body level spacing

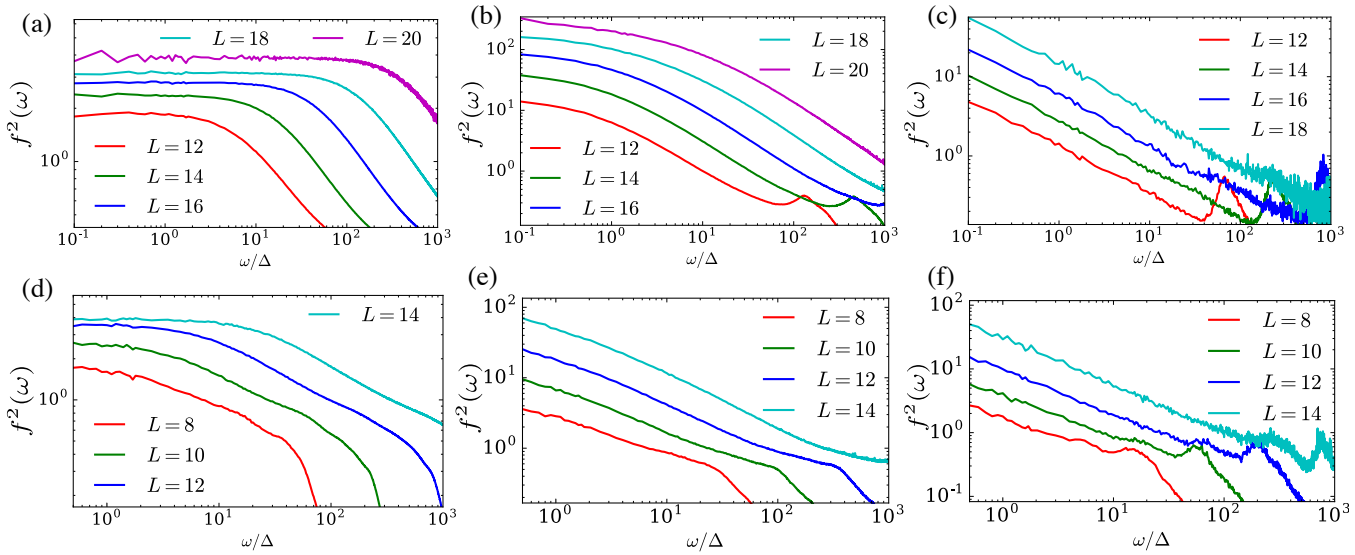

Figure 3. Plotting $f^2(\omega)$ as a function of ω/Δ reveals its behavior at very low energies. Top row [(a)-(c)]: XXZ model. (a) For weak disorder $W = 1$, the plateau in $f^2(\omega)$ for $\omega < E_{\rm Th}$ is followed by the power-law decay. (b) For intermediate disorder $W = 2$, the plateau fails to fully develop even for $L = 20$ spins, which signals that $E_{\rm Th} \sim \Delta$. (c) In the MBL phase $W = 5$, $f^2(\omega)$ decays as a power-law even for $\omega < \Delta$. Bottom row [(d)-(f)]: Ising model. Average $f^2(\omega)$ as a function of ω/Δ shows a developed plateau only for $\Gamma = 0.95$ (d). For stronger disorder [$\Gamma = 0.7$, (e)] the concave part is visible only for $L = 14$ spins. Finally, in the MBL phase at $\Gamma = 0.4$ (f) the spectral function decays as a power-law for all system sizes.

$\Delta \approx W\sqrt{L}/\mathcal{D}$, where $\mathcal{D}(L)$ is the Hilbert space dimension. For example, in the XXZ spin chain $\mathcal{D}(L) = \binom{L}{L/2}$, and in the Ising model $\mathcal{D}(L) = 2^L$. The rescaling of the horizontal axis by Δ displaces curves in Fig. 3 towards right with increasing L, hence the evolution of the Thouless energy is best visualized by comparing curves with the same L in different panels of Fig. 3.

The top row of Fig. 3 [(a)-(c)] shows the results for XXZ model. Deep in the ergodic phase, Fig. 3(a), the behavior of $f^2(\omega)$ is fully consistent with the expectations discussed above, see Eq. (6). In particular, the matrix elements do not depend on the energy difference, corresponding to the saturation of the spectral function to a constant for energies $\omega \lesssim E_{\rm Th}$, where $E_{\rm Th}$ is almost $1000 \times \Delta$ for $L = 20$ spins.

Notably, $E_{\rm Th}$ rapidly decreases as we increase the disorder strength. In particular, already for $W = 2$ (still far from the MBLT at $W_c \approx 3.75$), Fig. 3(b) illustrates the absence of a fully developed plateau for the largest studied system sizes. The concave form of $f^2(\omega)$ for ω near Δ persists through the MBLT up to disorder $W \lesssim 4$. At even stronger disorders, e.g., $W = 5$ in Fig. 3(c), the concave part of $f^2(\omega)$ entirely disappears, and $f^2(\omega)$ decays as a power-law for all $\omega < J_{\rm loc}$.

Bottom row of Fig. 3 [(d)-(f)] shows very similar behavior for the transverse field Ising model, i.e., upon increasing the disorder strength the Thouless energy disappears. This illustrates the fact that the disappearance of the plateau in the spectral function is a generic feature that precedes the MBLT. For example, already at disorder strength $\Gamma = 0.7$, when the parameter $\langle r \rangle$ is still much closer to its Wigner-Dyson value, the spectral function fails to develop a plateau, see Fig. 3(e). Below we systematically explore the variation of $E_{\rm Th}$ and power ϕ across the MBLT.

B. Thouless energy

To extract $E_{\rm Th}$ from the functional form of $f^2(\omega)$, we use the following fitting form:

$$f^2(\omega) = \frac{f^2(0)}{1 + (\omega/E_{\rm Th})^{\phi}}. \tag{12}$$

This ansatz is motivated by the asymptotic behavior in Eq. (6). The Thouless energy extracted from such fits for the XXZ model is shown in Fig. 4, where the dashed line corresponds to the diffusive ($\gamma = 1/2$) scaling of $E_{\rm Th} \propto 1/L^2$, and is consistent with the data for weak disorder $W = 1$.

Already for slightly bigger disorder $W = 1.5$, $E_{\rm Th}$ becomes comparable to the level spacing for the smallest system size $L = 12$. The fitting procedure and extraction of $E_{\rm Th}$ using ansatz (12) is still well-defined until $E_{\rm Th} \gtrapprox 0.1\Delta$. Nevertheless, in order to be interpreted as an inverse relaxation timescale of local observables, the Thouless energy must exceed the many-body level spacing. Hence, when $E_{\rm Th} \leq \Delta$ we expect that the inverse level spacing sets the relaxation timescale, whereas $E_{\rm Th}/\Delta < 1$ gives a probability that two nearby eigenstates are strongly mixed with each other. On the other hand, for disorder $W = 1.5$ the condition $E_{\rm Th} \geq \Delta$

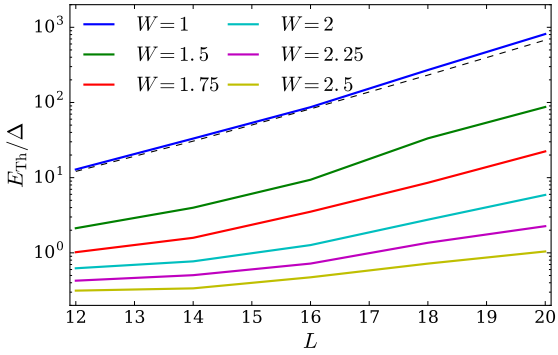

Figure 4. Thouless energy for the XXZ model at various disorders. The growth of $E_{\rm Th}/\Delta$ with L slows down as the value of the disorder is increased towards the MBLT. Already for $W = 2.5$ we have $E_{\rm Th} < \Delta$ even for $L = 20$. For larger disorders $E_{\rm Th}$ is too small to be reliably determined.

is quickly recovered with increasing system size with $E_{\rm Th}/\Delta \approx 100$ for $L = 22$ spins.

However, already at disorder $W \geq W_* \approx 2$, the growth of $E_{\rm Th}/\Delta$ becomes increasingly slower so that $E_{\rm Th}$ remains below the level spacing Δ for all available system sizes. While one cannot rule out the power-law behavior $E_{\rm Th} \propto L^{-1/\gamma}$ with very small γ, it is more natural to interpret this data as *exponential* dependence of $E_{\rm Th}$ with L, $E_{\rm Th} \propto e^{-\kappa L}$ with $\kappa < \ln 2$.

The smallness of $E_{\rm Th}$ and its exponential scaling indicate that our system enters a critical region near the MBLT. Recent phenomenological RG studies[21,22] suggested a logarithmic relaxation $L \sim \ln t$ in this region. Logarithmic growth of particle number fluctuations for $W < W_c$ was also demonstrated numerically.[46] If there exists a correlation length $\xi(W)$ that depends on disorder strength and diverges at the MBLT (when $W = W_c$), then even at disorder $W < W_c$ small systems of length $L \leq \xi(W)$ may qualitatively behave as if they were at the MBLT, so one has to study systems of size $L > \xi(W)$ to see the delocalized behavior. We note, that one should not confuse the divergent localization length $\xi(W)$ with the scale that governs the decay of different terms in the expansion of the local operator in terms of integrals of motion in the MBL phase. The latter scale always remains finite, even at the MBL transition.[42,46,51]

In this scenario, from Fig. 4 it follows that at $W_* \approx 2$, the correlation length $\xi(W_*) \geq 20$ exceeds our largest system size. Refs. 21 and 22 suggested scaling $\gamma \sim 1/\xi(W)$.[52] This implies $E_{\rm Th} \sim e^{-\alpha\xi(W)\ln L}$. From here, ignoring $\ln L$ in the exponent, one obtains that $E_{\rm Th}$ becomes much smaller than the level spacing $\sim e^{-L\ln 2}$ when $\xi(W) \gg L$, which matches the condition for being in the critical fan. For the fixed value of disorder, as soon as system size is larger than the correlation length $L > \xi(W)$, we expect to return to regime $E_{\rm Th}/\Delta \gg 1$. Assuming subdiffusive dynamics, in this regime $E_{\rm Th}$ should be decreasing as a power-law with L.

C. Power-law decay of spectral function

Additional evidence for the critical behavior comes from the decay of averaged spectral functions, $f^2(\omega)$, as well as the log-averaged ("typical") spectral function defined in Eq. (11). In Fig. 5 we show the power ϕ extracted from fitting $f^2(\omega)$ to Eq. (12) (red lines) and ϕ_{typ} which governs the decay of log-averaged spectral function (blue lines). Details of the fitting procedure are given in Appendix A.

In the XXZ model [Fig. 5, top] for disorders $0.5 < W < W_*$, the powers ϕ_{av} and ϕ_{typ} coincide. Moreover, $1/2 < \phi_{typ} \approx \phi < 1$. This is consistent with the subdiffusion observed numerically in the studies of different correlation functions in the time domain,[23–27] also Refs. 28 and 51 directly addressed the conductivity in the frequency domain. At the same time, we do not resolve the finite size flow of ϕ, so we cannot exclude that subdiffusion is a finite size effect, as suggested by other studies.[53–55]

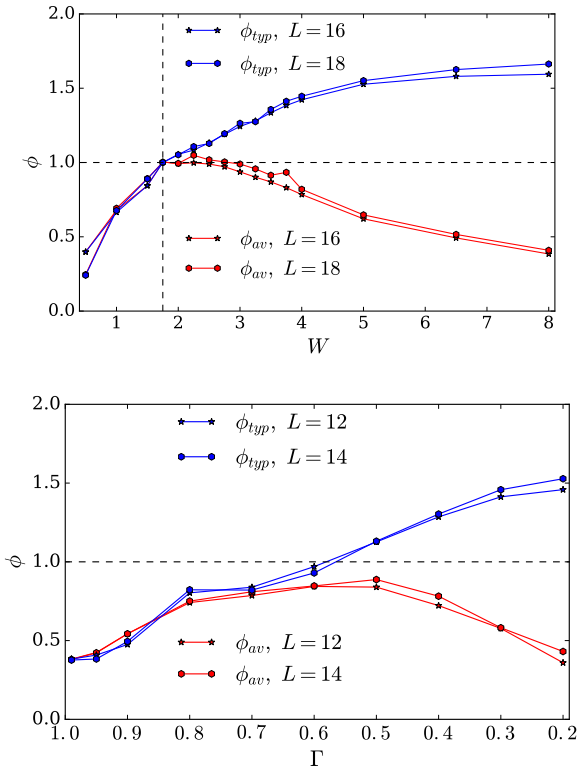

Figure 5. Powers ϕ_{av} and ϕ_{typ} controlling the decay of $f^2(\omega)$ and $[f^2(\omega)]_{\rm typ}$. Top: XXZ model where the powers saturate to one near $W_* \approx 2$. At larger disorder, ϕ_{av} decreases again, while ϕ_{typ} grows above one. Bottom: similar results for the Ising model, where the powers start to systematically deviate from each other for $\Gamma \leq 0.7$. This coincides with the disappearance of last traces of the Thouless plateau in $f^2(\omega)$ in the panel Fig. 3(e).

For $W \approx W_*$, both powers ϕ, ϕ_{typ} are close to one for some range of the disorder values, corresponding to $f^2(\omega)$ decaying as $1/\omega$. Via relation (4) this translates into a logarithmic decay of correlation functions in time, consistent with the critical region behavior. Note, that the saturation of the exponents ϕ and ϕ_{typ} to one holds only for the σ_1^z operator, which corresponds to the density of a conserved quantity in the XXZ model. For example, Fig. 9 in the Appendix demonstrates that the exponents ϕ, ϕ_{typ} for a different operator saturate at a value less than one before they start to deviate from each other.

Finally, for strong enough disorder $W > W_*$, ϕ and ϕ_{typ} do not agree anymore. This means that the average and typical matrix elements at a given energy difference are not only very different from each other, but they also depend on the energy difference in qualitatively distinct ways. This signals that the function $f^2(\omega)$ ceases to be smooth. Hence, we expect that the relation of ϕ to the exponent γ, governing the decay of the correlation functions with time, no longer holds. By contrast, in the regime where $f^2(\omega)$ is a smooth function, we expect $\gamma = 1 - \phi$, which follows from Eq. (4). Similar breakdown of typicality when $\phi < \phi_{typ}$ happens also for the spectral function of the spin flip operator in the XXZ chain (see Fig. 9 in the Appendix).

We interpret the disagreement between the exponents governing the decay of average and typical spectral functions as a signature that the average function $f^2(\omega)$ is dominated by rare resonances that give matrix elements of order one.[51] In contrast, the log-averaged spectral function is dominated by the most probable matrix elements, and $[f^2(\omega)]_{\rm typ}$ at fixed ω exponentially decreases with L, consistent with the criterion for the MBLT.[46]

The results for the Ising model, shown in the bottom panel of Fig. 5, are qualitatively similar to those of the XXZ model. The exponents ϕ are plotted as a function of the disorder strength Γ, for two largest system sizes $L = 12$ and 14. At weak disorder (large Γ), the average and log-averaged spectral function have identical exponents. At moderate disorders, the two exponent develop a plateau, beyond which they start to deviate from each other. This suggests that systems of $L = 14$ spins enter the critical regime at $\Gamma_* \approx 0.7$. We note that the plateau in this case occurs at a value $\phi < 1$. Comparing this with the data for spin flip operator shown in Fig. 9, we speculate that the plateau value $\phi = 1$ for σ_1^z operator in the XXZ spin chain may be related to the fact that this operator corresponds to the density of a conserved charge.

V. MULTIFRACTAL ANALYSIS

We now motivate the analysis of the matrix elements as amplitudes of a wave function. We consider a local perturbation represented by an operator $\hat{O}$ which acts on an eigenstate $|\alpha\rangle$. Then, the probability to find the system in the eigenstate $|\beta\rangle$ is given by

$$|O_{\alpha\beta}|^2 = |\psi_\alpha(\beta)|^2, \tag{13}$$

which can be interpreted as the squared wave function amplitude. If $\hat{O} \cdot \hat{O} = 1$, as is the case for $\hat{O} = \sigma_1^z$, this wave function is normalized, $\sum_\beta |\psi_\alpha(\beta)|^2 = 1$.

Although fractality was recently argued to be a generic property of many-body ground states,[56] fractal properties depend on the choice of the basis. Moreover, as suggested in Ref. 56, even trivial product state may get a "fractal" statistics of the wave function amplitudes in the improperly chosen basis. Nevertheless, Refs. 57 and 58 studied the decomposition of excited many-body eigenstates in the standard basis of product states and observed significant changes across the MBLT.

Here, in contrast to the above approaches, we relate the fractal dimensions in the eigenbasis of the unperturbed Hamiltonian to the onset of criticality and localization. This removes the ambiguity related to the choice of the basis. While our approach is potentially capable of extracting the wave function coefficients in the basis of product states, this would require to consider the operator $\hat{O}$ that projects all spins onto a given direction. In contrast, below we consider *local* operator that affects only a few spins.

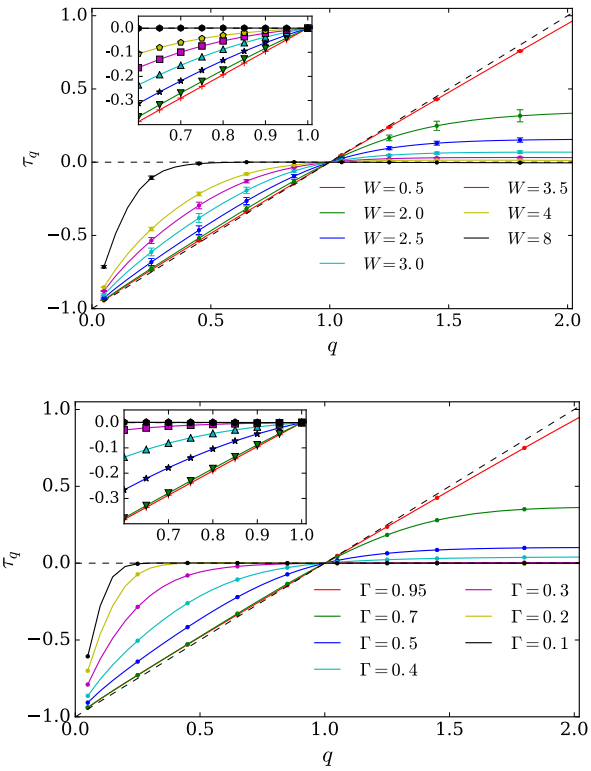

Figure 6. The multifractal spectrum τ_q in Eq. (15) as a function of the disorder strength, W for the XXZ model (top panel) and Γ for the Ising model (bottom panel). The spectrum evolves from being very close to that of a metal (red lines) to the "frozen" fractal spectrum deep in the MBL phase (black line). Inset shows τ_q near $q \leq 1$.

More specifically, to access the fractal properties of the matrix elements, we study q-th participation ratios of the wave function in Eq.(13),

$$P_q = \sum_\beta \langle |\psi_\alpha(\beta)|^{2q} \rangle, \tag{14}$$

where the brackets denote averaging over disorder and eigenstates α from a narrow band around the energy $E = 0$. The scaling of P_q with the Hilbert space dimension $\mathcal{D}$ is given by

$$P_q = \sum_\beta \langle |O_{\alpha\beta}|^{2q} \rangle \propto \frac{1}{\mathcal{D}^{\tau_q}}, \tag{15}$$

which defines the scaling dimension τ_q. We note, that in contrast to ALT, where participation ratios can be in principle probed in tuneling experiments, the relation of the above P_q to physical properties is not clear.

In Fig. 6 we directly calculate τ_q using ED data, since the SI data do not provide a complete set of matrix elements. We concentrate on τ_q as it suffers from fewer numerical issues, compared to the fractal spectrum $f(\alpha)$ related to τ_q via the Legendre transform.[59] If the distribution of matrix elements is very narrow, all $|\psi(\beta)|^2 \propto 1/\mathcal{D}$, and one expects $\tau_q = q-1$. At weak disorder, the scaling dimension for the matrix elements of $O = \sigma_i^z$ are indeed close to $q-1$, as shown by dashed lines in Fig. 6. The top panel of Fig. 6 is for the XXZ model and the bottom panel is for the Ising model. In both cases, at weak disorder ($W = 0.5$ for the XXZ model and $\Gamma = 0.95$ for the Ising model), the multifractal exponent indeed is very close to the expected $\tau_q = q - 1$. Note that the scaling dimensions necessarily obey $\tau_0 = -1$ and $\tau_1 = 0$, which are fixed by the dimension of the Hilbert space and the normalization of the wave function.

Upon increasing the disorder, the spectrum τ_q begins to deviate from $q-1$ for $q > 1$. The saturation of τ_q to a constant for $q > 1$ corresponds to the termination of the fractal spectrum of $f(\alpha)$.[59] This implies that the probability to find an amplitude of the wave function arbitrarily close to one scales as $1/\mathcal{D}^c$, with c given by the saturation value of τ_q. In the delocalized phase $c > 0$ and this probability vanishes in the thermodynamic limit, corresponding to rare occurrences of large matrix elements when $\hat{O}$ acts within rare localized "patches" of the system.

Finally, approximately when the system enters the MBL phase, all $\tau_q = 0$ for $q > q_f$, with $q_f < 1$. Such a spectrum of τ_q corresponds to the so-called "frozen" phase[59–61] combining properties of localized and critical states. In this case there is a *finite* probability of matrix elements being close to one, so a small number of large matrix elements (corresponding to local excitations) saturates the sum $\sum_\beta |O_{\alpha\beta}|^2 \approx 1$. This agrees with the picture of the MBL phase as being one where local perturbations have local effect.[12] In the Ising model, the freezing transition happens at $0.4 > \Gamma_c > 0.3$. This is consistent with the estimates of the MBLT from the level statistics given in Fig. 1 above; this estimate is also close to estimates for the MBLT in the Floquet model of Ref. 48.

In the MBL phase the form of τ_q with $q < 1$ probes the behavior of increasingly smaller matrix elements which do have non-trivial structure, despite being exponentially suppressed in the system size.[46] Note, our numerical results are in apparent disagreement with studies of the fractality of matrix elements within perturbation theory,[62] which suggest the scaling dimensions at the MBLT transition to be $\tau_q = 2q - 1$ for $q \leq 1/2$, similar to the case of the ALT in infinite dimension.[59]

VI. DISCUSSION

As mentioned in the Introduction, the Thouless energy is one of the central concepts in the theory of the ALT. In the single particle case the Thouless energy can be defined from the stiffness with respect to twisting boundary conditions.[20] In addition, the Thouless energy can be extracted from the overlap of different wave functions at the same point but at different energy.[30,31] In this work we introduced a many-body generalization of the Thouless energy defined instead via the spectral function, and studied it for two models with many-body localization transition.

For XXZ spin chain and transverse-field Ising model we extracted the Thouless energy as an energy scale at which the matrix elements of a local perturbation cease to depend on the energy difference.[63] Such a plateau in the spectral function physically corresponds to the energy scale below which the system becomes effectively zero-dimensional and where the random matrix theory applies. This definition of the Thouless energy may be viewed as a generalization of the single-particle definition studied in the context of single particle localization and random matrix models.[30,31] However, the important difference is that the spectral function has a richer structure, e.g. it is constrained to decay exponentially at large energy differences.[50]

The many-body Thouless energy reveals a broad critical regime preceding the MBLT. In the case of the disordered Heisenberg spin chain, this region starts from $W_* \approx 2$ for the largest accessible system size ($L = 20$) and is characterized by

(i) the simultaneous "shrinking" of the Thouless energy to a value below the many-body level spacing,

(ii) non-smooth spectral function $f^2(\omega)$, with different exponents governing the decay of averaged and log-averaged $[f^2(\omega)]_{typ}$, and

(iii) the multifractal behavior when the scaling dimensions of the participation ratios τ_q begin to deviate from the value in a metal, both at $q > 1$ and $q < 1$.

In addition, the MBLT approximately agrees with the onset of the frozen fractal spectrum. We note that these

conclusions hold for both generic local operators, as well as for operators that correspond to a conserved quantity. In addition, we found similar features (i)–(iii) in the disordered Ising model, where the only conserved quantity is total energy. These results suggest that the above features should be universal near MBLTs in various one-dimensional models.

The identified critical region is "broad" in the sense that for the system sizes accessible by ED and other numerical techniques, it starts at disorder that is much weaker than the disorder where the MBLT is believed to occur. For instance, the XXZ spin chains with $L = 20$ spins show critical behavior for $W_* \geq 2$, while the MBLT is expected to occur for $W_c \approx 3.75$. The discovered onset of broad distributions and the breakdown of self-averaging in the critical region suggests that one must exercise care in averaging quantities related to the matrix elements and the dynamics of the system.

On the other hand, the finite size scaling of the critical region suggests that it decreases with L. For instance, the Thouless energy in Fig. 4 monotonically increases with L even when the system is in the critical region. This is consistent with the existence of a localization length $\xi(W)$, which diverges at the MBLT when $W = W_c$, as suggested by renormalization group approaches.[21,22] The fact that this region shrinks with increasing L strongly suggests a direct transition between thermal and MBL phases. While the system sizes studied in the present work preclude the scaling analysis of $\xi(W)$, the larger-size numerics utilizing the SI method could potentially allow for such studies.

In addition, we note that our work complements recent numerical studies of the XXZ spin chain dynamics in the time domain.[24] While real-time dynamics can be performed for systems of up to $L \approx 30$ spins, the large system size limits the accessible evolution times. On the other hand, our study of the spectral function $f^2(\omega)$ for small energy separations $\omega \sim \Delta$ corresponds to long-time dynamics, hence it is complimentary to the numerical simulations of quantum dynamics in real time. It would be interesting to check if the breakdown of self-averaging and the onset of broad distributions has an analogue in the real time dynamics near the MBLT.

In the broader perspective, the signatures of the critical behavior in the microscopic models with a MBLT revealed here can be potentially useful as constraints on the phenomenological and random-matrix type models aiming to capture the physics of the MBLT. In particular, the matrix elements of local operators correspond to a perturbation that can be used to "stitch" together the initially disconnected systems, hence being relevant in the context of real-space renormalization group studies.

Appendix A: Numerical procedure and fitting of the spectral function

Here we provide additional details on the numerical procedure used to extract the spectral function. We use the weighted histogram for the differences of eigenenergies with weights given by the square of the corresponding matrix elements. Afterwards, the averaging is performed both over individual eigenstates in a narrow window near $E = 0$, as well as over different disorder realizations. For SI data the number of extracted eigenvalues is 1000, whereas for ED data the number of used eigenstates is chosen according to $\min(1000, \mathcal{D}/L)$, so it always corresponds to sub-extensive energy variation. In order to show the global structure of $f^2(\omega)$, the bin width of the weighted histogram is fixed at a small value that is larger than the level spacing for the smallest system $L = 10$. For the plots of $f^2(\omega/\Delta)$, the energy difference is divided by the average level spacing, and the histogram bin size is equal to one level spacing. When we extract the typical value of the spectral defined in Eq. (11) and shown in Fig. 2, the *logarithm* of the absolute value of

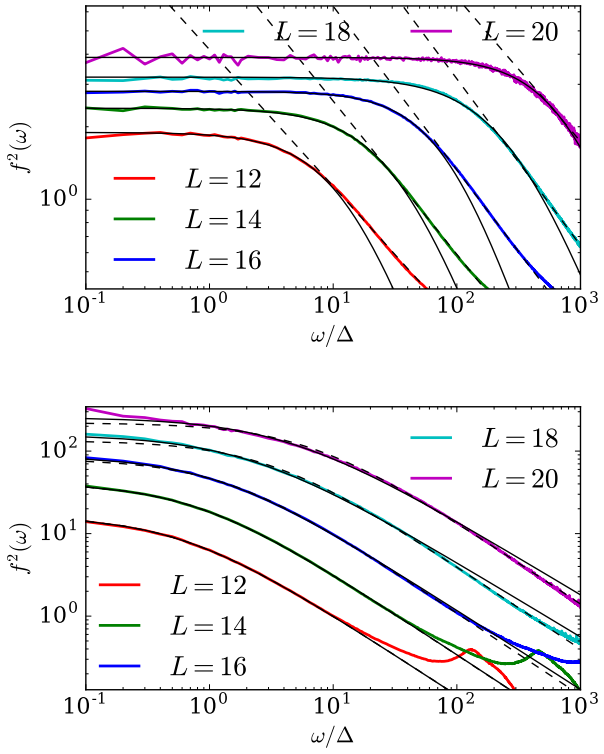

Figure 7. Illustration of the fits quality of $f^2(\omega)$ in the XXZ model for $W = 1$ (top panel) and $W = 2$ (bottom panel). Note that Eq. (5) fails to capture the onset of decay of $f^2(\omega)$ at weak disorder in the top panel, thus we fitted the data with the power-law (straight dashed lines). Dashed lines denote fits used to extract the power ϕ, whereas solid lines were used to determine $E_{\rm Th}$ and $f^2(0)$.

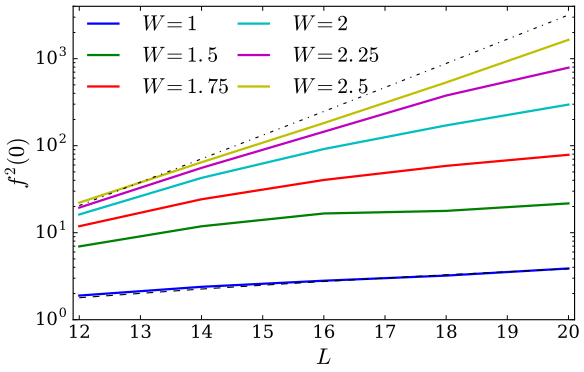

Figure 8. Dependence of $f^2(0)$ in the XXZ model on L for different values of the disorder. For weak disorder, the data is consistent with the power-law dependence of $E_{\rm Th}$ on the system size (the bottom dashed line corresponds to diffusive behavior). Upon increasing the disorder, $f^2(0)$ gets enhanced, but still grows slower that $1/\Delta$ which is illustrated by the top dot-dashed line.

matrix element is used as weight.

In order to demonstrate our fitting procedure, in Fig. 7 we show the fits used to extract the power ϕ and the Thouless energy. We see that at $W = 1$, Eq. (5) fails to adequately capture the decay of $f^2(\omega)$. Therefore, for disorders $W = 1$ and $W = 1.5$ we extracted ϕ by fitting the "shoulder" to the power-law behavior, as is illustrated by dashed lines in the top panel of Fig. 7. However, already for disorder $W \geq 1.75$, Eq. (5) adequately describes the behavior of $f^2(\omega)$. In particular, the bottom panel of Fig. 7 shows excellent agreement between $f^2(\omega)$ and its fits by Eq. (5). For all values of the disorder $W \geq 1.75$ we used fits of $f^2(\omega)$ to extract the Thouless energy and $f^2(0)$. In order to capture the power-law decay more accurately, we fitted $\ln f^2(\omega)$ to the logarithm of Eq. (5); the corresponding fits are shown by dashed lines in the bottom panel of Fig. 7.

Appendix B: Energy dependence of the matrix elements

We show the magnitude of spectral function at the small energies, $f^2(0)$, extracted from the fits of $f^2(\omega)$ in Fig. 8. Its behavior with system size is consistent with the dependence of $E_{\rm Th}$ on L, shown in Fig.4 in the main text. Indeed, if one assumes that the equilibrium expectation value of $\hat{O}$ is exponentially small in the system size, $f^2(\omega)$ obeys the sum rule. Then, provided that the sum rule is dominated by the contributions from small frequencies, the saturation value $f^2(0)$ can be related to the finite size scaling of $E_{\rm Th}$.[40] More specifically, from $E_{\rm Th} \propto L^{-1/\gamma}$ we get $f^2(\omega) \propto L^{1/\gamma-1}$, i.e., the value of the spectral function at the plateau grows with the system size in a power-law fashion. In contrast, if the Thouless energy is comparable to the level spacing, we expect that $f^2(\omega)$ scales with the inverse level spacing, as is the case in Fig. 8 for larger values of the disorder.

We note that this suggests an alternative interpretation of the results in recent Ref. 44. Our Fig. 8 suggests that while the power-law scaling of $\mathrm{std}(O_{\alpha\beta}e^{S/2})$ holds at weak disorder, for stronger disorder within the critical region (i.e., for $W \geq W_*$), the exponential dependence $\mathrm{std}(O_{\alpha\beta}e^{S/2}) \propto e^{\alpha L}$ is more natural. We expect this exponential dependence to crossover into the power-law when the system size becomes larger than the correlation length. Such a crossover is visible for $W = 1.5$ and $W = 1.75$ curves in Fig. 8. However, upon approaching the MBLT the correlation length diverges and there will be progressively larger range of system sizes where this exponential dependence is observed. The exponential dependence of $E_{\rm Th}$ on L may explain a strong upward curvature of $\mathrm{std}(O_{\alpha\beta}e^{S/2})$ plotted as a function of L on the double logarithmic scale in Fig. 3 of Ref. 44.

Finally, Fig. 9 is a plot of the exponent governing the power-law decay for the matrix elements of the operator $\sigma_1^x\sigma_2^x + \sigma_1^y\sigma_2^y$. Similar to the matrix elements of σ^z operator, shown in Fig. 5, the power ϕ in Fig. 9 has a plateau as a function of W before the exponents governing the typical and average spectral function deviate from each other. Note, however, that in contrast to the operator σ^z, in the present case the power ϕ_{av} never reaches one.

Appendix C: Fractal properties of matrix elements

Our data for the scaling dimension τ_q, Fig. 6, illustrated the presence of fractality even at very moderate disorders. Here we address the finite size scaling of these scaling dimensions: Fig. 10 shows τ_q extracted from smaller (dashed lines) and larger (solid lines) system sizes.

While τ_q consistently deviates below $q - 1$ for $q > 1$, even at disorder $W = 0.5$, we see a strong flow of τ_q with

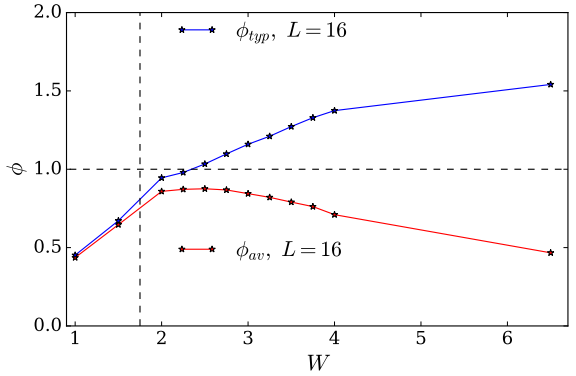

Figure 9. Average and typical exponents ϕ governing the decay of $f^2(\omega)$ in the XXZ model for the operator $\sigma_1^x\sigma_2^x + \sigma_1^y\sigma_2^y$. The results are similar to Fig. 5 where the operator was σ_1^z.

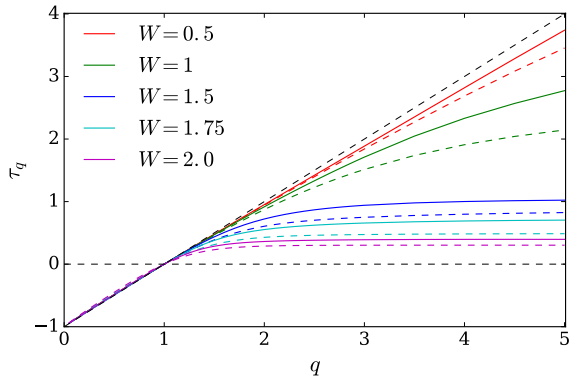

Figure 10. The finite size flow of τ_q in the XXZ model (for operator $\hat{O} = \sigma_1^z$). The solid lines show τ_q using data for $L = 10 \dots 16$, while dashed lines are extracted using $L = 8 \dots 14$. Note that while τ_q always flows to metallic asymptote for with increasing system size, this flow becomes hardly noticeable for $W \geq 2$.

system size, and τ_q becomes closer to $q - 1$ for larger system sizes. In contrast, when the disorder approaches W_*, i.e., when the system is in the critical region near the MBLT, the finite size flow of τ_q becomes hardly noticeable. This supports the conclusion that the fractal behavior of the matrix elements is pertinent to the wide critical region surrounding the MBLT.

Next, we address the fractality for the case of a different operator – namely we consider the operator $\sigma_1^x\sigma_2^x + \sigma_1^y\sigma_2^y$, which flips the spins at two adjacent sites when they point in opposite directions. While such an operator no longer squares to the identity, Fig. 11 demonstrates that the condition $\tau_1 = 0$ still holds, i.e., that the squared sum of the matrix elements $\sum_\beta O_{\alpha\beta}^2$ does not depend on the system size. In addition, Fig. 11 support the assertion that the flow of the scaling dimensions is universal and does not depend on the specific form of the operator. While the operator σ_1^z corresponds to the local density of a global conserved quantity (total spin), the operator $\sigma_i^x\sigma_{i+1}^x + \sigma_i^y\sigma_{i+1}^y$ does not have such a special property. Nevertheless, its scaling dimensions behave similarly to the case of σ^z operator: τ_q weakly deviates from the metallic behavior at weak disorder. Upon increasing the disorder, τ_q saturates for some $q > 1$ consistent with the termination of the fractal spectrum. For disorder $W \geq 4$ (in the MBL phase) we also observe the characteristic "frozen" spectrum.

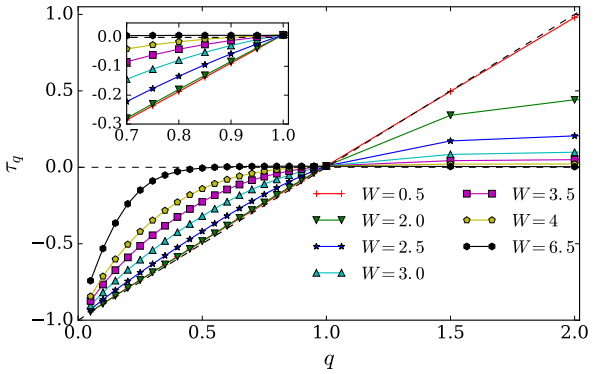

Figure 11. Scaling dimension for the operator $\hat{O} = \sigma_1^x\sigma_2^x + \sigma_1^y\sigma_2^y$, in the XXZ model.

Finally, we also present the distribution of the participation ratio of the matrix elements of the operator σ^z in Fig. 12. At weak disorder, the width of the distribution shrinks, consistent with τ_q approaching the limit $q - 1$ of the ideal metal. However, already at disorder $W = 1$ we observe an approximately scale invariant form of the above distribution, with the power-law decay of the probability to have large participation ratios $p(P_2/P_2^{typ}) \propto 1/P_2^{1+x_2}$. For $W = 1$ we have $x_2 \approx 2$. Exponent x_2 decreases for increasing the disorder, and it is close to 1 already for $W = 1.5$. Note that when $x_2 < 1$, the scaling dimension extracted from P_2 begins to deviate from the "typical" scaling dimension extracted from the log-averaged participation ratio, see Ref. 59 for more details. Finally, at even stronger disorder, $W = 2$, the distribution of the participation ratios loses its scale invariant form and begins to broaden for larger systems.

ACKNOWLEDGMENTS

We acknowledge useful discussions with V. Kravtsov, T. Grover, and R. Vasseur. M.S. was supported by Gordon and Betty Moore Foundation's EPiQS Initiative through Grant GBMF4307. Z.P. acknowledges support by EPSRC grant EP/P009409/1. Statement of compliance with EPSRC policy framework on research data: This publication is theoretical work that does not require supporting research data. M.S. and D.A. acknowledge hospitality of KITP, where parts of this work were completed (supported in part by the National Science Foundation under Grant No. NSF PHY11-25915).

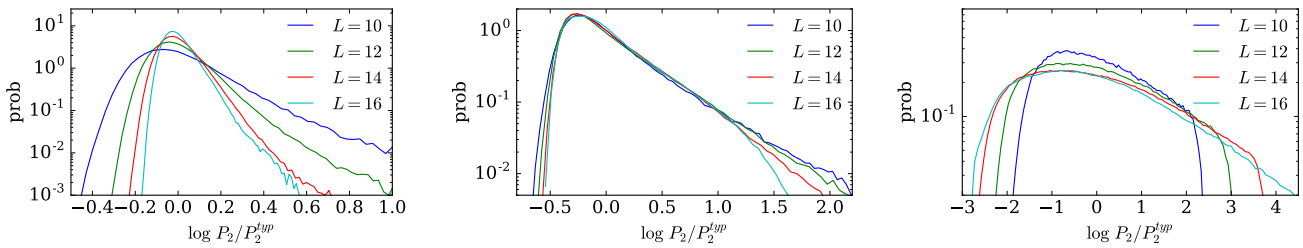

Figure 12. Distribution of participation ratios P_2 on the ergodic side of the MBLT in the XXZ model. For weak disorder, $W = 0.5$ (left), the distribution becomes increasingly narrower for larger systems. However, already at disorder $W = 1$ (middle) the distribution looks scale-invariant, with the power law decay of probability to have $P_2 > P_2^{typ}$. Finally, at even stronger disorder $W = 2$ (right), the distribution consistently broadens with the system size.

[1] A. Polkovnikov, K. Sengupta, A. Silva, and M. Vengalattore, *Colloquium : Nonequilibrium dynamics of closed interacting quantum systems,* Rev. Mod. Phys. **83**, 863–883 (2011).

[2] J. M. Deutsch, Phys. Rev. A **43**, 2146 (1991).

[3] M. Srednicki, *Chaos and quantum thermalization,* Phys. Rev. E **50**, 888–901 (1994).

[4] M. Rigol, V. Dunjko, and M. Olshanii, *Thermalization and its mechanism for generic isolated quantum systems,* Nature **452**, 854–858 (2008).

[5] M. Srednicki, *Thermal fluctuations in quantized chaotic systems,* Journal of Physics A: Mathematical and General **29**, L75 (1996).

[6] M. Srednicki, *The approach to thermal equilibrium in quantized chaotic systems,* Journal of Physics A: Mathematical and General **32**, 1163 (1999).

[7] D. Basko, I. Aleiner, and B. Altshuler, *Metal–insulator transition in a weakly interacting many-electron system with localized single-particle states,* Annals of Physics **321**, 1126 – 1205 (2006).

[8] I. V. Gornyi, A. D. Mirlin, and D. G. Polyakov, *Interacting electrons in disordered wires: Anderson localization and low-t transport,* Phys. Rev. Lett. **95**, 206603 (2005).

[9] V. Oganesyan and D. A. Huse, *Localization of interacting fermions at high temperature,* Phys. Rev. B **75**, 155111 (2007).

[10] A. Pal and D. A. Huse, *Many-body localization phase transition,* Phys. Rev. B **82**, 174411 (2010).

[11] B. Bauer and C. Nayak, *Area laws in a many-body localized state and its implications for topological order,* Journal of Statistical Mechanics: Theory and Experiment **2013**, P09005 (2013).

[12] M. Serbyn, Z. Papić, and D. A. Abanin, *Local conservation laws and the structure of the many-body localized states,* Phys. Rev. Lett. **111**, 127201 (2013).

[13] D. A. Huse, R. Nandkishore, and V. Oganesyan, *Phenomenology of fully many-body-localized systems,* Phys. Rev. B **90**, 174202 (2014).

[14] M. Znidaric, T. Prosen, and P. Prelovsek, *Many-body localization in the heisenberg xxz magnet in a random field,* Phys. Rev. B **77**, 064426 (2008).

[15] J. H. Bardarson, F. Pollmann, and J. E. Moore, *Unbounded growth of entanglement in models of many-body localization,* Phys. Rev. Lett. **109**, 017202 (2012).

[16] M. Serbyn, Z. Papić, and D. A. Abanin, *Universal slow growth of entanglement in interacting strongly disordered systems,* Phys. Rev. Lett. **110**, 260601 (2013).

[17] M. Serbyn, Z. Papić, and D. A. Abanin, *Quantum quenches in the many-body localized phase,* Phys. Rev. B **90**, 174302 (2014).

[18] J. Z. Imbrie, *On many-body localization for quantum spin chains,* Journal of Statistical Physics **163**, 998–1048 (2016).

[19] V. Ros, M. Müller, and A. Scardicchio, *Integrals of motion in the many-body localized phase,* Nuclear Physics B **891**, 420 – 465 (2015).

[20] J. T. Edwards and D. J. Thouless, *Numerical studies of localization in disordered systems,* Journal of Physics C: Solid State Physics **5**, 807 (1972).

[21] R. Vosk, D. A. Huse, and E. Altman, *Theory of the many-body localization transition in one dimensional systems,* ArXiv e-prints (2014), arXiv:1412.3117 [cond-mat.dis-nn].

[22] A. C. Potter, R. Vasseur, and S. A. Parameswaran, *Universal properties of many-body delocalization transitions,* Phys. Rev. X **5**, 031033 (2015).

[23] K. Agarwal, S. Gopalakrishnan, M. Knap, M. Müller, and E. Demler, *Anomalous diffusion and griffiths effects near the many-body localization transition,* Phys. Rev. Lett. **114**, 160401 (2015).

[24] D. J. Luitz, N. Laflorencie, and F. Alet, *Extended slow dynamical regime close to the many-body localization transition,* Phys. Rev. B **93**, 060201 (2016).

[25] Y. Bar Lev, G. Cohen, and D. R. Reichman, *Absence of diffusion in an interacting system of spinless fermions on a one-dimensional disordered lattice,* Phys. Rev. Lett. **114**, 100601 (2015).

[26] V. Kerala Varma, A. Lerose, F. Pietracaprina, J. Goold, and A. Scardicchio, *Energy diffusion in the ergodic phase of a many body localizable spin chain,* ArXiv e-prints (2015), arXiv:1511.09144 [cond-mat.dis-nn].

[27] M. Žnidarič, A. Scardicchio, and V. K. Varma, *Diffusive and subdiffusive spin transport in the ergodic phase of a many-body localizable system,* Phys. Rev. Lett. **117**, 040601 (2016).

[28] O. S. Barišić, J. Kokalj, I. Balog, and P. Prelovšek, *Dynamical conductivity and its fluctuations along the*

crossover to many-body localization, Phys. Rev. B **94**, 045126 (2016).
[29] I. Khait, S. Gazit, N. Y. Yao, and A. Auerbach, *Spin transport of weakly disordered heisenberg chain at infinite temperature,* Phys. Rev. B **93**, 224205 (2016).
[30] E. Cuevas and V. E. Kravtsov, *Two-eigenfunction correlation in a multifractal metal and insulator,* Phys. Rev. B **76**, 235119 (2007).
[31] V. E. Kravtsov, I. M. Khaymovich, E. Cuevas, and M. Amini, *A random matrix model with localization and ergodic transitions,* New Journal of Physics **17**, 122002 (2015).
[32] F. Wegner, *Inverse participation ratio in 2+ϵ dimensions,* Zeitschrift für Physik B Condensed Matter **36**, 209–214 (1980).
[33] C. M. Soukoulis and E. N. Economou, *Fractal character of eigenstates in disordered systems,* Phys. Rev. Lett. **52**, 565–568 (1984).
[34] C. Castellani and L. Peliti, *Multifractal wavefunction at the localisation threshold,* Journal of Physics A: Mathematical and General **19**, L429 (1986).
[35] F. Evers, A. Mildenberger, and A. D. Mirlin, *Multifractality of wave functions at the quantum hall transition revisited,* Phys. Rev. B **64**, 241303 (2001).
[36] A. Rodriguez, L. J. Vasquez, K. Slevin, and R. A. Römer, *Critical parameters from a generalized multifractal analysis at the anderson transition,* Phys. Rev. Lett. **105**, 046403 (2010).
[37] E. Khatami, G. Pupillo, M. Srednicki, and M. Rigol, *Fluctuation-dissipation theorem in an isolated system of quantum dipolar bosons after a quench,* Phys. Rev. Lett. **111**, 050403 (2013).
[38] R. Steinigeweg, J. Herbrych, and P. Prelovšek, *Eigenstate thermalization within isolated spin-chain systems,* Phys. Rev. E **87**, 012118 (2013).
[39] W. Beugeling, R. Moessner, and M. Haque, *Off-diagonal matrix elements of local operators in many-body quantum systems,* Phys. Rev. E **91**, 012144 (2015).
[40] L. D'Alessio, Y. Kafri, A. Polkovnikov, and M. Rigol, *From quantum chaos and eigenstate thermalization to statistical mechanics and thermodynamics,* Advances in Physics **65**, 239–362 (2016).
[41] C. L. Bertrand and A. M. García-García, *Anomalous thouless energy and critical statistics on the metallic side of the many-body localization transition,* Phys. Rev. B **94**, 144201 (2016).
[42] R. Nandkishore, S. Gopalakrishnan, and D. A. Huse, *Spectral features of a many-body-localized system weakly coupled to a bath,* Phys. Rev. B **90**, 064203 (2014).
[43] M. Serbyn and J. E. Moore, *Spectral statistics across the many-body localization transition,* Phys. Rev. B **93**, 041424 (2016).
[44] D. J. Luitz and Y. Bar Lev, *Anomalous thermalization in ergodic systems,* ArXiv e-prints (2016), arXiv:1607.01012 [cond-mat.stat-mech].
[45] D. J. Luitz, N. Laflorencie, and F. Alet, *Many-body localization edge in the random-field heisenberg chain,* Phys. Rev. B **91**, 081103 (2015).
[46] M. Serbyn, Z. Papić, and D. A. Abanin, *Criterion for many-body localization-delocalization phase transition,* Phys. Rev. X **5**, 041047 (2015).
[47] X. Chen, T. Zhou, D. A. Huse, and E. Fradkin, *Out-of-time-order correlations in many-body localized and thermal phases,* Annalen der Physik , 1600332–n/a (2016), 1600332.
[48] L. Zhang, V. Khemani, and D. A. Huse, *A floquet model for the many-body localization transition,* Phys. Rev. B **94**, 224202 (2016).
[49] V. Hernandez, J. E. Roman, and V. Vidal, *SLEPc: A scalable and flexible toolkit for the solution of eigenvalue problems,* ACM Trans. Math. Software **31**, 351–362 (2005).
[50] D. A. Abanin, W. De Roeck, and F. m. c. Huveneers, *Exponentially slow heating in periodically driven many-body systems,* Phys. Rev. Lett. **115**, 256803 (2015).
[51] S. Gopalakrishnan, M. Müller, V. Khemani, M. Knap, E. Demler, and D. A. Huse, *Low-frequency conductivity in many-body localized systems,* Phys. Rev. B **92**, 104202 (2015).
[52] The assumption in Refs. 21 and 22 is that the subdiffusive dynamics outside of the critical region is related to the Griffiths regions of size $r \sim \xi \log L$ which have exponential tunneling time, $t \sim e^{cr}$, one arrives at $t_* \sim L^{c\xi}$. Matching this to $L \sim t_*^{\gamma}$ one obtains that the exponent γ governing the decay of correlation functions vanishes as $\gamma \sim 1/\xi(W)$.
[53] R. Steinigeweg, J. Herbrych, F. Pollmann, and W. Brenig, *Typicality approach to the optical conductivity in thermal and many-body localized phases,* Phys. Rev. B **94**, 180401 (2016).
[54] S. Bera, G. De Tomasi, F. Weiner, and F. Evers, *Density propagator for many-body localization: finite size effects, transient subdiffusion, (stretched-)exponentials,* ArXiv e-prints (2016), arXiv:1610.03085 [cond-mat.str-el].
[55] P. Prelovšek, M. Mierzejewski, O. Barišić, and J. Herbrych, *Density correlations and transport in models of many-body localization,* ArXiv e-prints (2016), arXiv:1611.03611 [cond-mat.str-el].
[56] D. J. Luitz, F. Alet, and N. Laflorencie, *Universal behavior beyond multifractality in quantum many-body systems,* Phys. Rev. Lett. **112**, 057203 (2014).
[57] A. De Luca and A. Scardicchio, *Ergodicity breaking in a model showing many-body localization,* Europhys. Lett. **101**, 37003 (2013).
[58] E. J. Torres-Herrera and L. F. Santos, *Dynamics at the many-body localization transition,* Phys. Rev. B **92**, 014208 (2015).
[59] F. Evers and A. D. Mirlin, *Anderson transitions,* Rev. Mod. Phys. **80**, 1355–1417 (2008).
[60] C. d. C. Chamon, C. Mudry, and X.-G. Wen, *Localization in two dimensions, gaussian field theories, and multifractality,* Phys. Rev. Lett. **77**, 4194–4197 (1996).
[61] Y.-Z. Chou and M. S. Foster, *Chalker scaling, level repulsion, and conformal invariance in critically delocalized quantum matter: Disordered topological superconductors and artificial graphene,* Phys. Rev. B **89**, 165136 (2014).
[62] C. Monthus, *Many-body-localization transition: strong multifractality spectrum for matrix elements of local operators,* Journal of Statistical Mechanics: Theory and Experiment **7**, 073301 (2016), arXiv:1603.04701 [cond-mat.dis-nn].
[63] We note, that the stiffness of the many-body eigenenergies with respect to twisting boundary conditions in the many-body case is related to the sum of matrix elements of current operator, see Ref. 64, and thus it is not clear if the single-particle relation between stiffness and Thouless energy can be generalized to the many-body case.
[64] M. Filippone, P. W. Brouwer, J. Eisert, and F. von Oppen, *Drude weight fluctuations in many-body localized systems,* ArXiv e-prints (2016), arXiv:1606.07291 [cond-mat.mes-

hall].